Virologica Sinica (2020) 35:156–170
https://doi.org/10.1007/s12250-019-00164-7

www.virosin.org
www.springer.com/12250

RESEARCH ARTICLE

Structural Basis of Glycan Recognition in Globally Predominant Human P[8] Rotavirus

Xiaoman Sun[1,2] · Lei Dang[1,2,3] · Dandi Li[1,2] · Jianxun Qi[4] · Mengxuan Wang[1,2] · Wengang Chai[5] · Qing Zhang[1,2] · Hong Wang[1,2] · Ruixia Bai[3] · Ming Tan[6] · Zhaojun Duan[1,2]

Received: 25 July 2019 / Accepted: 21 August 2019 / Published online: 16 October 2019

Abstract

Rotavirus (RV) causes acute gastroenteritis in infants and children worldwide. Recent studies showed that glycans such as histo-blood group antigens (HBGAs) function as cell attachment factors affecting RV host susceptibility and prevalence. P[8] is the predominant RV genotype in humans, but the structural basis of how P[8] RVs interact with glycan ligands remains elusive. In this study, we characterized the interactions between P[8] VP8*s and glycans which showed that VP8*, the RV glycan binding domain, recognized both mucin core 2 and H type 1 antigens according to the ELISA-based oligosaccharide binding assays. Importantly, we determined the structural basis of P[8] RV-glycans interaction from the crystal structures of a Rotateq P[8] VP8* in complex with core 2 and H type 1 glycans at 1.8 Å and 2.3 Å, respectively, revealing a common binding pocket and similar binding mode. Structural and sequence analysis demonstrated that the glycan binding site is conserved among RVs in the P[II] genogroup, while genotype-specific amino acid variations determined different glycan binding preference. Our data elucidated the detailed structural basis of the interactions between human P[8] RVs and different host glycan factors, shedding light on RV infection, epidemiology, and development of anti-viral agents.

Keywords Rotavirus (RV) · P[8] · Glycan binding specificity · VP8* structure · Mucin core 2 · Lacto-N-fucopentaose 1 (LNFP1)

Introduction

Rotaviruses (RVs) are a major cause of acute gastroenteritis in infants and young children, claiming about 215,000 lives worldwide annually (Tate *et al*. 2016). RVs are non-enveloped, double stranded RNA (dsRNA) viruses with 11 dsRNA segments encoding 12 proteins (Estes and Greenberg 2013). Each RV virion is composed of three concentric capsid layers. The outermost layer consists of the glycoprotein VP7 and the protease-sensitive spike protein VP4, which define the RV G and P genotypes, respectively (Matthijnssens *et al*. 2011). RVs are genetically diverse, consisting of at least 35 G and 50 P genotypes identified so far (https://rega.kuleuven.be/cev/viralmetagenomics/virus-classification/rcwg). VP4 can be cleaved by trypsin into two proteins, VP5* and VP8*, and VP8* interacts with cell surface carbohydrates for RV attachment (Fiore *et al*. 1991). Based on the VP8* sequences, the diverse P genotypes have been grouped into five genogroups (P[I]–P[V]) (Huang *et al*. 2012). P[4], P[6], P[8], and P[19] genotypes are grouped into P[II]

Xiaoman Sun, Lei Dang, Dandi Li and Jianxun Qi have contributed equally to this work.

✉ Zhaojun Duan
zhaojund@126.com

1 National Health Commission Key Laboratory for Medical Virology and Viral Diseases, Beijing 102206, China

2 National Institute for Viral Disease Control and Prevention, China CDC, Beijing 102206, China

3 Inner Mongolia Medical University, Huhehaote 010059, China

4 Institute of Microbiology, Chinese Academy of Sciences, Beijing 100101, China

5 Glycosciences Laboratory, Department of Medicine, Imperial College London, London, UK

6 Division of Infectious Diseases, University of Cincinnati College of Medicine, Cincinnati, OH, USA

genogroup, among which P[8] RVs are the most widely circulating human RVs (Yu *et al.* 2018). Several live-attenuated RV vaccines, including Rotateq® (Merck) and Rotarix® (GSK) that contain P[8] genotype, have been implemented in many countries, which has reduced the RV infection associated mortality and morbidity significantly (Rha *et al.* 2014; Burnett *et al.* 2018; Pindyck *et al.* 2018). Despite these advancements, the current vaccines do not show satisfactory efficacy in many developing countries and the reason for this low efficacy remain unknown (Desselberger 2017). Thus, further study for the better understanding of RV-host interaction, RV infection, and prevalence is necessary for improved control and prevention strategies to reduce mortality and morbidity caused by RVs.

Recognition of the cellular receptors is a crucial step in virus infection and is a major determinant of viral host range, tissue tropism, and epidemiology. VP8*, the RV carbohydrate-receptor binding protein, plays an important role in the initial cell attachment and recognizes glycan ligands in a genotype-dependent manner (Ruggeri and Greenberg 1991; Tan and Jiang 2014; Jiang *et al.* 2017). Some animal RVs were reported to be sialidase-sensitive previously, while human RVs were sialidase-insensitive (Ciarlet and Estes 1999; Kuhlenschmidt *et al.* 1999; Haselhorst *et al.* 2009). Histo-blood group antigens (HBGAs) have been demonstrated to be cell attachment factors for some human RVs based on structural and functional evidence (Hu *et al.* 2012; Huang *et al.* 2012; Liu *et al.* 2012), while mucin cores also interact with some human and animal RV VP8*s (Liu *et al.* 2016; Sun *et al.* 2016d; Pang *et al.* 2018). Both mucin cores and HBGAs are O-linked glycans that are synthesized by a group of glycosyltransferases. Four common core structures (core 1–4) constitute the majority O-glycans of mucins, such as human intestinal mucins that distribute abundantly on the epithelial cell surface, building up the intestinal mucus (Jensen *et al.* 2010). HBGAs are expressed on the red blood cells and epithelial cells at the mucosal surfaces and are also present in biological fluids, such as mucosal secretions, saliva, and milk. HBGAs are synthesized by sequential addition of monosaccharide to the disaccharide precursors with a β1,3 and β1,4 linkage and are highly polymorphic including the ABO, secretor (H), and Lewis families (Skovlund 1997; Tan and Jiang 2014), which may significantly affect RV epidemiology.

Several epidemiological studies have indicated an association between the polymorphic human HBGAs and susceptibility of RV infections. For example, human P[8] and P[4] RVs infected preferably Lewis positive secretors, while P[6] RVs could infect both Lewis positive and Lewis negative individuals (Nordgren *et al.* 2014; Van Trang *et al.* 2014). Further studies documented that non-secretors phenotype appear to be associated with resistance to severe gastroenteritis caused by P[8] RVs (Imbert-Marcille *et al.* 2014; Gunaydin *et al.* 2016; Zhang *et al.* 2016; Pollock *et al.* 2018). However, P[8] RV infection was also found in non-secretor individuals (Ayouni *et al.* 2015; Sun *et al.* 2016b). A recent study showed that the polymorphism of human HBGAs was associated with susceptibility to RVs. Nonetheless, *in vitro* infection of transformed cells appeared to be independent of HBGA expression (Barbe *et al.* 2018). These scenarios indicate the complexity in the interactions between RVs and various glycans, as well as the complex roles of HBGAs in human RVs infection, which needs to be further explored.

Human P[14], P[9], and P[25] RVs in the P[III] genogroup have been demonstrated to interact with A type HBGA (Hu *et al.* 2012; Liu *et al.* 2012), while human P[11] RVs in the P[IV] genogroup recognized type 1 and type 2 precursors (Liu *et al.* 2013; Ramani *et al.* 2013). Human P[4] and P[8] RVs were shown previously to interact with H1 and Lewis b antigens (Huang *et al.* 2012; Ma *et al.* 2015). Later, Liu *et al.* (2016) reported that VP8* of P[19] RV in the same P[II] genogroup bound to mucin core 2/4/6 and type 1 glycans. They also found that human P[4] and P[8] recognized mucin core 2, while human P[6], another P[II] genotype, did not bind to mucin core 2 but interacted with H type 1 precursor glycan lactose-N-tetrarose (LNT) (Liu *et al.* 2016). In addition, a study using nuclear magnetic resonance (NMR) spectroscopy indicated interaction between human P[8] RV (Wa strain) VP8* and GM1/GD1a (Haselhorst *et al.* 2009) and Wa RV was reported to recognize GM1 ganglioside during cellular infection (Fleming *et al.* 2014). Another study using saturation transfer difference (STD) NMR spectroscopy showed that type A HBGAs may be receptors for human P[4] RV DS-1 strain and P[6] RV-3 strain, but not P[8] Wa strain (Bohm *et al.* 2015). Thus, the RV-glycan interactions are complicated, particularly how the most prevalent P[8] RVs interact with the glycan ligands remains elusive.

Crystallography is a powerful tool to illustrate the detailed interactions and structural basis between RV VP8* and its glycan receptors. The crystal structure of P[14] HAL1166 VP8* complexed with type A-HBGA showed that the A-antigen binding site shares the same location as the sialic acid binding site in a Rhesus P[3] RV VP8* at one corner of the cleft region between the two β-sheets (βH and βK) (Dormitzer *et al.* 2002; Hu *et al.* 2012). The crystal structure of human P[11] N155 VP8* in complex with lactose-N-tetrarose (LNT) or lactose-N-neotetrarose (LNnT) revealed a larger glycan binding pocket beside the one of P[14] HAL1166, spanning almost the entire length of the cleft (Hu *et al.* 2015). The glycan binding pocket in P[19] appears to be unique compared with the other known ones, being located adjacent to the cleft and formed mainly

by a 169–172 loop and a 209–212 loop (Liu *et al*. 2017; Sun *et al*. 2018). The crystal structures of human P[4] Indian and P[6] RV3 VP8*s complexed with type 1 glycan Lacto-N-fucopentaose 1 (LNFP1) have been solved recently, revealing the same glycan binding sites as that of P[19] VP8* (Hu *et al*. 2018). The crystal structures of P[8] Wa and Rotateq VP8* alone have been determined previously (Blanchard *et al*. 2007; Sun *et al*. 2016a). In this study, we further characterized the glycan binding specificity of P[8] RV VP8*s and determined the crystal structures of Rotateq P[8] VP8* complexed with mucin core glycan and H type 1 antigen, providing a structural basis for the P[8] RV-glycan ligand interactions.

Materials and Methods

VP8* Proteins Expression and Purification

VP8* genes (residues 1–231) of Rotateq P[8] (GenBank: GU565044), P[8]BEL(GenBank: JN849151) were synthesized in Genewiz (Suzhou, China) and cloned into the pGEX4T-1 vector. Human P[6] (5311142) (GenBank: KT162986), human P[4] (11151099) (GenBank: KT162987), human P[8]lab (11221075) (GenBank: KT162984) were described previously (Ma *et al*. 2015). Recombinant VP8* proteins with N-terminal GST-tag were expressed in *E. coli* BL21 (DE3) cells (Tiangen) as previously described (Sun *et al*. 2016a). GST-fusion VP8*s were purified with Glutathione beads (GE healthcare) using established procedures (Sun *et al*. 2016a). VP8* core (residues 64-223) fragment of Rotateq P[8] was cloned into the pET30a vector and expressed in *E.coli* with C-terminal his-tag. VP8* core protein was purified with HiTrap Fast Flow (GE healthcare). Further purification was performed with gel filtration using superdex 200 column with 20 mmol/L Tris–HCl (pH 8.0), 50 mmol/L NaCl. The concentration of the purified protein was determined by the BCA Kit (BD Biosciences) with 2 mg/mL BSA as a standard.

ELISA-Based Oligosaccharide Binding Assay

Oligosaccharide binding assay was carried out as previously reported (Sun *et al*. 2016a). GST fusion VP8* proteins were coated on the 96 well plate (Costar) at 100 μg/well at 4 °C overnight. After blocking with 5% non-fat milk, PAA-biotin labeled oligosaccharides (including mucin core 2, mucin core 4, mucin core 6, LNT, H type 1, H type 2, A, B, Lewis a, Lewis b) were added at two concentrations 0.2 and 1 μg/well respectively. The plate was left at 4 °C overnight. Horseradish peroxidase-conjugated streptavidin (Abcam) was then added at 0.1 μg/well after washing the plates 5 times with phosphate-buffered saline (PBS)-0.05% Tween 20. The reactions were conducted using a 3,3′,5,5′-tetramethylbenzidine kit (BD Biosciences) and the absorbance of 450 nm was measured. The experiment was repeated twice and samples were performed with duplicates each time.

Crystallization

The Rotateq P[8] VP8* core protein in buffer (20 mmol/L Tris-HCl, 50 mmol/L NaCl, pH 8.0) was concentrated to approximately 20 mg/mL and crystallized using the sitting-drop vapor diffusion method at 18 °C with 1 μL of protein mixed with 1 μL of reservoir solution. Crystals were grown under the condition of 0.1 mol/L sodium acetate trihydrate pH 4.5, 2.0 mol/L ammonium sulfate. In order to obtain the protein-glycan complex, the glycans core 2 or LNFP1 were co-crystallized with the VP8* protein. The threonine-linked core 2 trisaccharide was prepared from Fmoc-protected peracetylated core 2-Thr (Sussex Research Laboratories, Ottawa, Canada) after deprotection (Johannes *et al*. 2015). Core 2-Thr was purified by high-performance liquid chromatography (HPLC) and analyzed by electrospray ionization mass spectrometry (ESI-MS) before use. The pentasaccharide Lacto-N-fucopentaose 1 (LNFP1) was purchased from Dextra Laboratories (UK). VP8* and core 2/LNFP1 were co-crystallized using a protein/ligand ratio of 1:50/1:200, respectively, under the same conditions as for the native crystal described above.

Data Collection, Processing, and Structure Determination

Crystals were dipped briefly in cryoprotectant solution containing 20% (v/v) glycerol and then flash-frozen in liquid nitrogen. Diffraction data were collected at the Shanghai Synchrotron Radiation Facility BL17U. Data were processed using HKL2000 software (Otwinowski and Minor 1997). The structures were solved by molecular replacement using Phaser software (Read 2001) with the structure of Rotateq P[8] VP8* (Protein Data Bank [PDB] ID: 5JDB) as the search model (Sun *et al*. 2016a). The initial model was refined using REFMAC5, COOT, and PHENIX software (Emsley and Cowtan 2004; Adams *et al*. 2010). The structural analysis was carried out with the PyMOL software package (https://pymol.org/2/). The statistical data for P[8] VP8*-core 2 and VP8*-LNFP1 are presented in Table 1. Protein structure accession numbers: the structures of P[8] VP8*-core 2 and VP8*-LNFP1 have been deposited in PDB with the access codes of 6K2N and 6K2O, respectively.

Table 1 Crystallographic X-ray diffraction and refinement statistics.

Parameter[a]	RotaTeq P[8] VP8*-Core 2	RotaTeq P[8] VP8*-LNFP1
Data collection		
Space group	$P2_1$	$P6_322$
Cell dimensions		
a, *b*, *c* (Å)	66.289	80.454
	114.55	80.454
	73.789	116.593
α, β, γ (°)	90, 95.959, 90	90, 90, 120
Wavelength (Å)	0.97774	0.97852
Resolution (Å)	50.00–1.80	50.00–2.30
	(1.86–1.8)	(2.38–2.30)
R_{merge} (%)[b]	8.4 (80.4)	15.9 (86.0)
$I/\sigma I$	21.597 (1.500)	22.524 (4.889)
Completeness (%)	98.4 (90.3)	99.57 (96.58)
Redundancy	5.4 (5.4)	25.8 (27.0)
Refinement		
Resolution (Å)	43.24–1.80	44.71–2.30
No. reflections	86599	10481
R_{work}/R_{free}	0.2024/0.2288	0.2035/0.2331
No. atoms		
Protein	7860	1336
Ligand/ion	80	52
Water	781	80
B-factors		
Protein	23.5	31.1
Ligand	59.8	74.7
Water	34.4	39.6
R.m.s. deviations		
Bond lengths (Å)	0.005	0.003
Bond angles (°)	0.69	0.54
Ramachandran plot		
Favored (%)	97.47	98.14
Allowed (%)	2.53	1.86
Disallowed (%)	0.00	0.00

[a]Values in parentheses are given for the highest resolution shell.

[b]Rmerge = Σhkl |I−< I>|/ΣhklI, where I is the intensity of unique reflection hkl and <I> is the average over symmetry-related observations of unique reflection hkl, hkl is the reflection indices.

Hemagglutination Assay

Human red blood cells (RBCs) of A, B, and O types and animal blood cells (Gelaidisi, Beijing) were washed twice with PBS before use and diluted to 1% RBCs. The GST-VP8* fusion proteins were twofold-serially diluted with 50 μL per well on 96-well V-bottom plates (Costar, Corning) and the original protein concentration was at 2 mg/mL. 50 μL of RBCs was added each well subsequently. The plate was incubated at 25 °C and agglutination was determined 1 h later. Wells without aggregates were considered as agglutination.

Virus Infection Inhibition Assay

We performed fluorescent focus assays on African green monkey kidney epithelial cells (MA104 cells) in the presence and absence of glycans, with infections in the absence of glycans considered to be 100% infectivity. The MA104 cells were seeded on the 96-well plate (Costar). Laboratory-adapted Wa (G1P[8]) and SA11 (G3P[2])

rotavirus strains were investigated. Dilutions of virus yielding ~200 focus forming units per well were preincubated for 30 min with media containing human milk, LNFP1, mucin core 2, lactose, or media without glycan. Human milk was used at 1:10. The glycans were tested at a final concentration of 1 mg/mL and 5 mg/mL (for LNFP1). The MA104 cells on the 96-well plate were washed twice with ice-cold serum-free 1640 medium. After cooling the cells and virus to 4 °C, the virus-milk or virus-glycan media were added and incubated on ice for 1 h. The inoculum was removed and cells were washed twice with ice-cold serum-free 1640 medium. The plates with serum-free 1640 medium were then put back in the incubator at 37 °C for 20 h. The cells were then fixed with ice cold methanol. Infected cells were detected with an anti-P[8] VP8* polyclonal rabbit serum (raised in-house, 1:400 dilution), followed by a fluorescein isothiocyanate (FITC)-conjugated goat anti-rabbit secondary antibody (Abcam, 1:1000 dilution).

Statistical Analysis

Data analysis was performed using SPSS software. Analysis of variance (ANOVA) with Dunnett's correction for multiple comparisons was used. Values of $P < 0.05$ were considered to indicate statistical significance.

Results

P[8] RV VP8*s Bound Mucin Core and H Type 1 Glycans

In order to define the interactions between P[8] RV VP8*s and various glycans (Fig. 1A), VP8* proteins of three different P[8] RV strains, including the vaccine strain of Rotateq, the predominant strain in China in 2014, referred as P[8] 11221075, and another P[8] strain in 2009 BEL were produced for glycan binding assays (Fig. 1B). All these P[8] VP8* proteins bound conclusively to mucin core 2 glycans (Fig. 1C, 1D). P[8] 11221075 VP8* showed weak binding signals to mucin core 4 and 6 oligosaccharides (Fig. 1C). P[8] 11221075 VP8* displayed obvious binding to H type 1 glycans. P[8] VP8*s bound to mucin core 2 and H type 1 glycans in a dose-dependent manner (Fig. 1D). In addition, human P[4] 11151099 and P[6] 5311142 VP8*s also bound mucin core 2 glycans. Human P[8] and P[4] VP8*s appeared not to bind LNT, while human P[6] VP8* did (Fig. 1C). No interaction was seen between P[8]/P[4] VP8*s and type A, B, Le^a, Le^b, and H type 2 antigens (Fig. 1C). As a positive control, P[14] VP8* bound A antigen.

Structural Basis of Rotateq P[8] VP8*-Core 2 Glycan Interaction

The crystal structure of Rotateq P[8] VP8* in complex with a core 2 trisaccharide was determined at the resolution of 1.8 Ångström (Å) (Fig. 2A). There were six protein molecules in the asymmetric unit. The electron density of core 2 were observed clearly in chain B and chain D. The core 2 trisaccharide of chain D was presented at 1 sigma level in the simulated annealing omit map (2mFo-DFc) (Fig. 2B). The residues W81, L167, Y169, G170, G171, R172, W174, T185, R209, and E212 of the VP8* protein participated in the interactions with the core 2 trisaccharide and thus build the cavity shaped glycan binding site (Fig. 2C). The edge of the glycan binding cavity is composed of the β-strand K, the I-J loop, and the 210 loop (residues 209–212), which links β-strand M and α-helix A; while the base of the binding cavity was formed by residues W81, L167, and W174. The core 2 trisaccharide was stabilized by a network of hydrogen bonds and hydrophobic interactions (Fig. 2C). The GlcNAc is the major binding saccharide forming four hydrogen bonds with T185, R209, E212, and four hydrophobic interactions with W81, L167, W174, T185, E212. In addition, the GalNAc formed two hydrogen bonds with R172 and two hydrophobic interactions with G170 and R172, while the Gal only formed hydrophobic interactions with Y169, G170, and G171.

Crystal Structure of Rotateq P[8] VP8* Complexed with H-Type 1 Glycan LNFP1

We also co-crystallized Rotateq VP8* in complex with an H type I pentasaccharide, Lacto-N-fucopentaose 1 (LNFP1, Fucα1-2Galβ1-3GlcNAcβ1-3Galβ1-4Glc) (Fig. 3A). The complex structure was determined at 2.3 Å resolution. There was one protein molecule in the asymmetric unit. The non-reducing end of LNFP1 was clearly seen at 1 sigma level of the electron density 2mFo-Fc map whereas the Gal moiety at the reducing end was not well-defined. Meantime, the Glc moiety at the reducing end were not shown because of the low map density (Fig. 3B). LNFP1 bound the VP8* protein at the same site as core 2 glycan. The residues W81, L167, Y169, G170, R172, W174, T184, T185, R209, E212, and N216 were involved in the interactions (Fig. 3C). The GlcNAcIII contributed mostly to the interactions by forming four hydrogen bonds with T185, R209, E212 and four hydrophobic interactions with W81, L167, W174, E212. The GalII at the non-reducing end interacted with T185 via a hydrogen bond and T184, T185, N216 through hydrophobic interactions, while Fuc-I was not involved in direct interactions. The GalIV at the reducing end further stabilized the glycan by forming three hydrophobic interactions with Y169, G170, and R172.

A

Glycans	Molecular Formula
mucin core2	Galβ1-3(GlcNAcβ1-6)GalNAcα-PAA-biotin
mucin core4	GlcNAcβ1-3(GlcNAcβ1-6)GalNAcα-PAA-biotin
mucin core6	GlcNAcβ1-6GalNAcα-PAA-biotin
H1	Fucα1-2Galβ1-3GlcNAcβ-PAA-biotin
H2	Fucα1-2Galβ1-4GlcNAcβ-PAA-biotin
Lewis a	Galβ1-3(Fucα1-4)GlcNAcβ-PAA-biotin
Lewis b	Fucα1-2Galβ1-3(Fucα1-4)GlcNAcβ-PAA-biotin
A tetra	GalNAcα1-3(Fucα1-2) Galβ1-4GlcNAcβ-PAA-biotin
B tetra	Galα1-3(Fucα1-2) Galβ1-4GlcNAcβ-PAA-biotin
LNT	Galβ1-3GlcNAcβ1-3Galβ1-4Glcβ-PAA-biotin
Core 2	Galβ1-3(GlcNAcβ1-6)GalNAc
LNFP1	Fucα1-2Galβ1-3GlcNAcβ1-3Galβ1-4GlcNAc

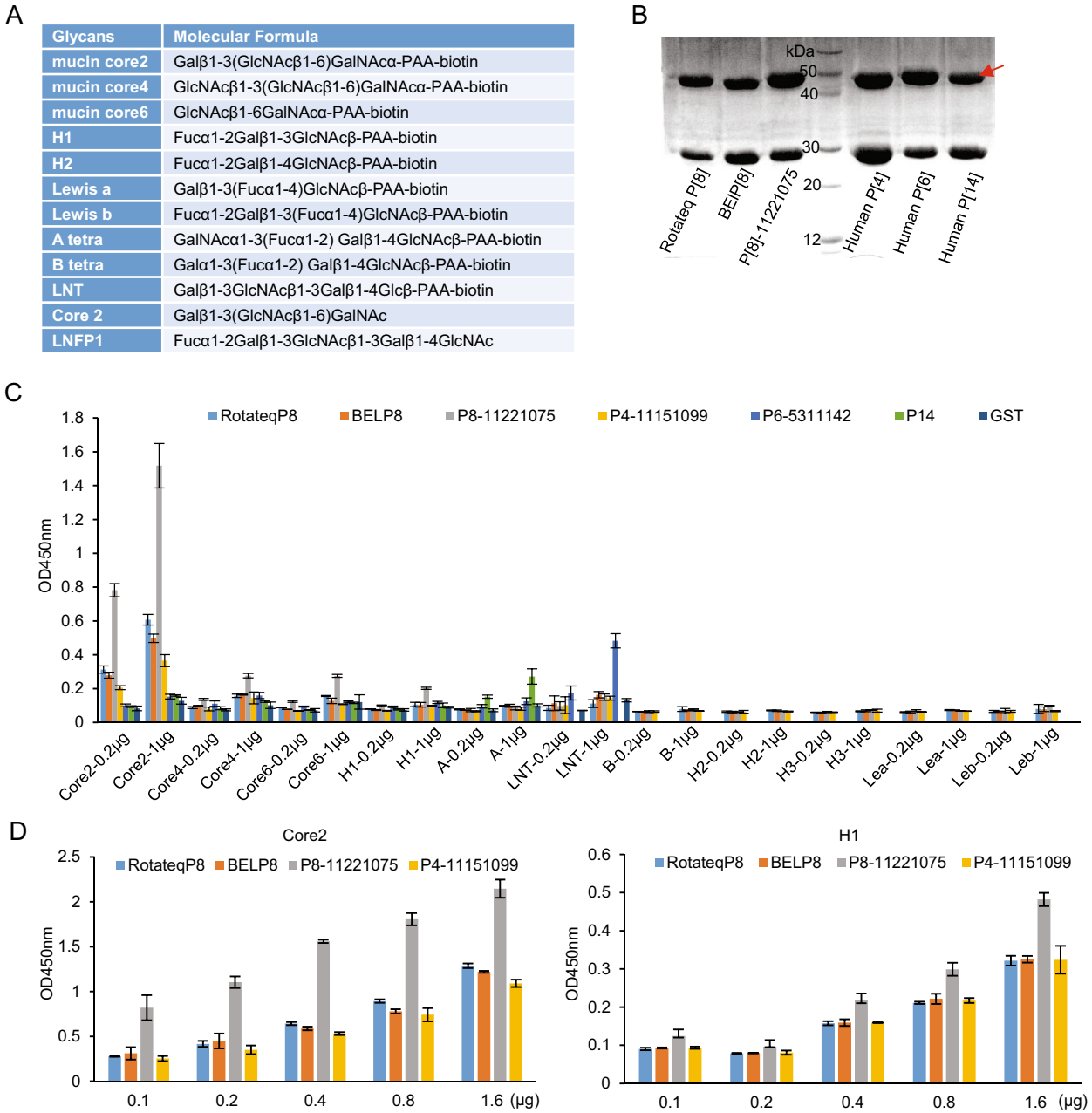

Fig. 1 Glycan binding assay of P[8] VP8*s. **A** The glycans involved in this study are listed. **B** The SDS-PAGE of the GST-VP8* fusion proteins (~52 kDa). Red arrow indicates the proteins of interest. The 26 kDa protein was free GST. **C** GST-VP8* proteins of Rotateq P[8], BElP[8], labP[8]-11221075, human P[4]-11151099, human P[6]-5311142, human P[14] were tested for the binding to oligosaccharides including core 2, core 4, core 6, H1, A, LNT (lactose-N-tetrarose, Galβ1-3GlcNAcβ1-3Galβ1-4Glc) at two concentrations (0.2 μg and 1 μg). Interactions with B, H1, H2, lewis a, lewis b were also performed for Rotateq P[8], BElP[8], labP[8]-11221075, and human P[4]-11151099. Human P[14] bound to A-HBGA was a positive control and GST protein was used as the negative control. **D** Rotateq P[8], BElP[8], P[8]-11221075, and human P[4]-11151099 bound to core 2 and H1 with a series of glycan concentrations (0.1, 0.2, 0.4, 0.8, 1.6 μg).

Structural Comparison of the Ligand Binding Sites Among Different RV VP8*s

Compared with the Rotateq VP8* structure (Sun *et al.* 2016a), glycan binding did not cause apparent conformational change, with the root mean squared deviation (RMSD) for alpha carbons of the backbone atoms between the bound VP8* and the free VP8* being 0.15 Å (mucin core 2) and 0.20 Å (LNFP I), respectively. Structural superimposition indicated that the core 2 trisaccharide and

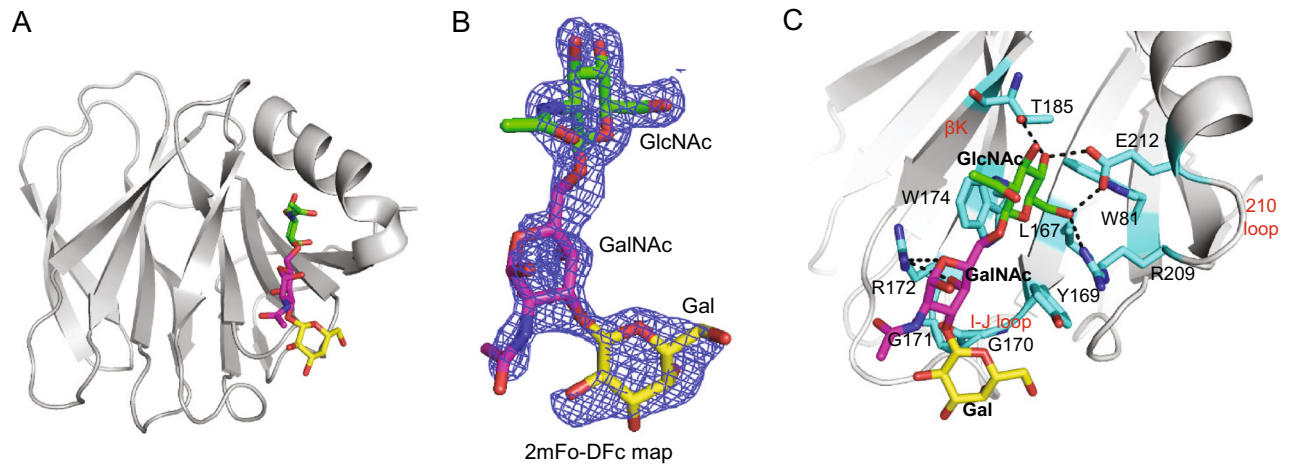

Fig. 2 Crystal structures of Rotateq P[8] VP8*-core 2 complex. **A** The cartoon representation of P[8] VP8*-core 2 complex structures. The monosaccharide residues of core 2 are shown in stick representation. **B** The 2mFo-DFc omit difference electron density map of core 2 in P[8] VP8* structure, contoured at 1σ level is shown. GlcNAc, green; GalNAc, magenta; Gal, yellow. **C** The detailed interactions between core 2 and VP8*. The monosaccharide residues of core 2 and amino acids involved in the interaction are shown in stick representation. The hydrogen bonds are presented with dashed lines. The interactions were searched for by CCP4 (http://ccp4.ac.uk/) with the distance of less than 5 Å and then calculated by PyMOL (https://pymol.org/2/).

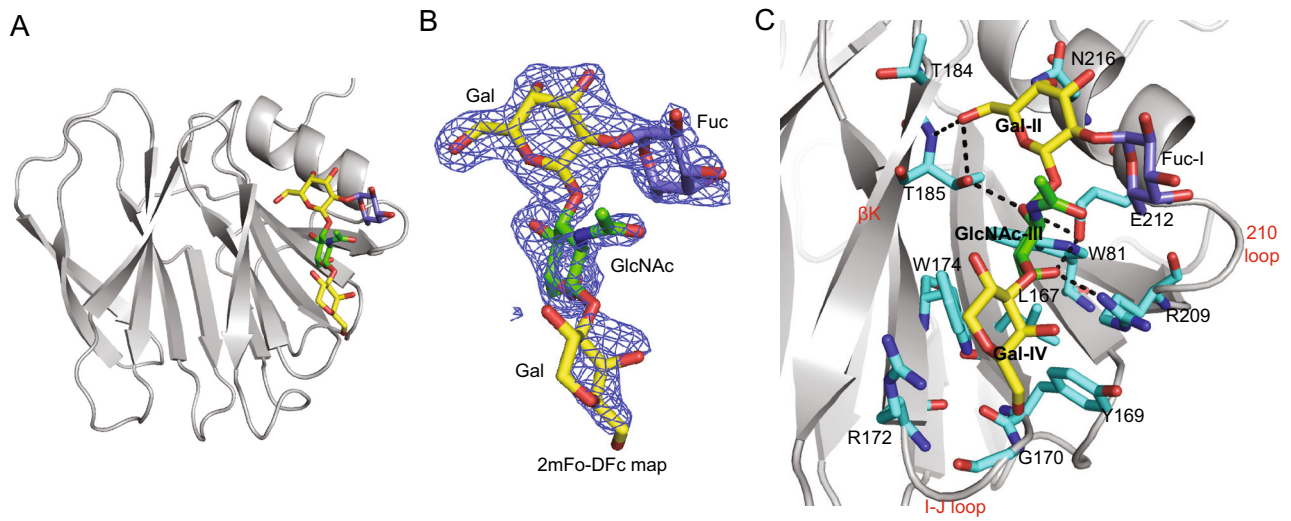

Fig. 3 Crystal structures of Rotateq P[8] VP8*-LNFP1 complex. **A** The cartoon representation of P[8] VP8*-LNFP1 complex structures. LNFP1 is shown in stick representation. **B** The 2mFo-DFc omit difference electron density map of LNFP1 in P[8] VP8* structure, contoured at 1σ level is shown. GlcNAc, green; Gal, yellow; Fuc, slate. **C** The detailed interactions between LNFP1 and VP8*. The hydrogen bonds are presented with dashed lines. The interactions were analyzed in the same way as described in the legend of Fig. 2C.

the LNFP1 pentasaccharide bound the same site of P[8] VP8*. There is a slight shift in the orientation of the GlcNAc moiety (pointed by a white arrow in Fig. 4A) between the bound mucin core 2 and the LNFP1 oligosaccharides, resulting in an orientation shift of the two glycan backbones within the binding cleft (Fig. 4A). In both cases, VP8* interacted with the glycans in a similar mechanism with the GlcNAc as the major interacting saccharide (Fig. 4B). Compared with the mucin core 2 trisaccharide, the LNFP1 pentasaccharide interacts with two additional residues, T184 and N216 of P[8] VP8* (Fig. 4B, 4C).

Structural analysis of the Rotateq P[8] VP8*-core 2 complex showed similar interaction mechanism as that seen in P[19] VP8*. Core 2 glycans lay at the same position of P[8] and P[19] VP8*s and interacted with the same set of amino acids except the residue 169 (Fig. 5A). Y169 in RotateqP[8] VP8* contributed a single hydrophobic interaction with Gal of the core 2 trisaccharide, whereas H169 in P[19] VP8* form two hydrophobic interactions with both GlcNAc and Gal (Fig. 5A).

The complex structures of the P[4] Indian, P[6] RV3, and P[19] VP8*s with LNFP1 have been determined and

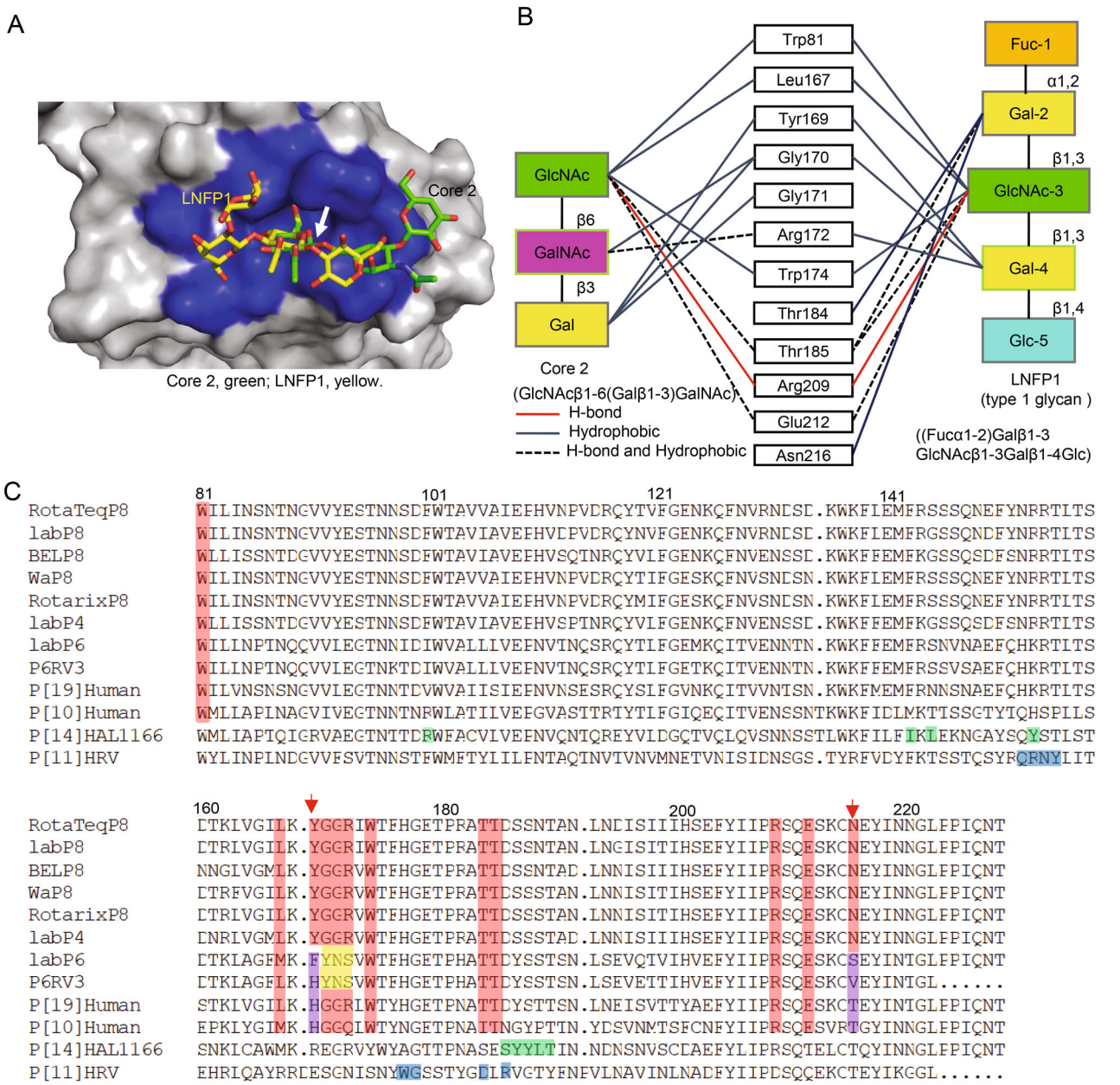

Fig. 4 Structural comparison of Rotateq P[8] VP8*-glycan structures. **A** Structure superimposition of Rotateq P[8] VP8*-core 2 and P[8] VP8*-LNFP1. Core 2/LNFP1 are shown in stick representation and colored green/yellow, respectively. The binding cavity is colored blue in the surface representation. The orientation of GlcNAc is highlighted by a white arrow. **B** Detailed presentation of the P[8] VP8*-glycans (core 2/LNFP1) interactions. Hydrogen bonding and hydrophobic interactions were shown. **C** Sequence alignment of VP8* of human RV P genotypes. Sequences of VP8* proteins (residues 81-231) among different human RV P genotypes were analyzed. The alignment was done with DNAMAN. The numbering of the amino acids was based on Rotateq VP8*. The amino acids involved in the glycan binding cavity of P[II] genogroup, P[14], P[11] were colored red, green, blue, respectively. The different residues participating in the glycan binding in human P[6] were highlighted in yellow. Residues 169 and 216 were pointed with red arrows and were colored purple in P[6] and P[19].

superimpositions of these structures showed that these VP8*s shared a common glycan binding site (Fig. 5B, 5C). The non-reducing end (Galβ1-3GlcNAc) of LNFP1 lay in the VP8*s via the same conformation, while Glc at the reducing end showed certain variations. For example, the Glc possesses a conformation closer to the binding cavity of P[6] VP8*, while the same Glc points away from the cavity of other VP8*s (Fig. 5B). The Fuc at the non-reducing end keeps a fixed orientation and was not involved in the direct interaction with the VP8*s. Sequence alignment showed that the amino acids that interact with the glycans, including W81, L167, Y169, G170, G171,

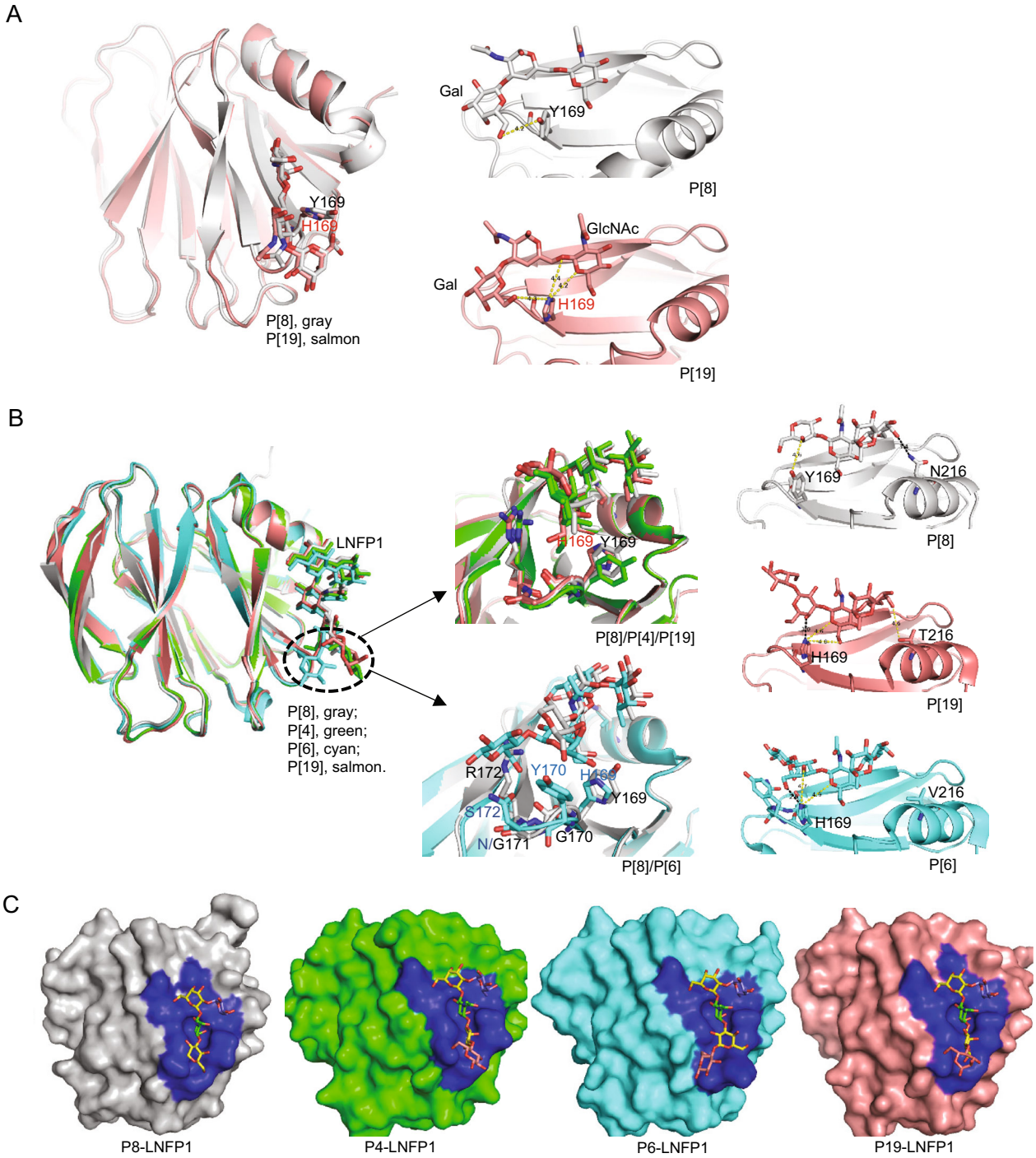

Fig. 5 Structural comparison of different P genotype VP8*s-glycan structures. **A** Structure superimposition of Rotateq P[8] VP8*-core 2 (grey), P[19]-core 2 (salmon) (PDB ID: 5YMS [Ref. (Liu *et al*. 2017)]), Y169 of P[8] and H169 of P[19] were shown in stick. The hydrophobic interactions were shown in yellow dot lines. **B** Structure superimposition of Rotateq P[8] VP8*-LNFP1 (grey), P[4]-LNFP1 (green) (PDB ID: 5VX5) [Ref. (Hu *et al*. 2018)], P[6]-LNFP1 (cyan) (PDB ID: 5VX9) [Ref. (Hu *et al*. 2018)], P[19]-LNFP1 (salmon) (PDB ID: 5VKS) [Ref. (Liu *et al*. 2017)]. Residue 169 of P[8]/P[4]/P[19] and residues 169-172 of P[8] and P[6] were shown in sticks in the middle panel. The interactions between LNFP1 and residue 169/216 in P[8]/P[19]/P[6] VP8* were shown in the right panel. Hydrophobic interactions were shown in yellow dashed lines and hydrogen bond was shown in black dashed line. **C** Detailed presentation of the LNFP1 binding pocket of P[8]/P[4]/P[6]/P[19] VP8*s. The binding cavity is colored blue in the surface representation. LNFP1 is shown in stick. GlcNAc, green; Gal, yellow; Fuc, slate, Glc, pink.

R172, W174, T184, T185, R209, E212, and N216, are relatively conserved in the P[8] and P[4] VP8*s, but variations were seen in P[19] and P[6], especially in P[6] VP8*, although its glycan binding site remains at the same location (Fig. 4C). The amino acids of H169, Y170, N171, and S172 in P[6] RV3 VP8* appeared to form stronger interactions with the Glc of LNFP1, bringing the glycan much closer to the binding cavity. Particularly, H169 in P[6] and P[19] VP8*s formed hydrogen bonds with Gal4 of LNFP1 (Fig. 5B), instead, Y169 in the P[4] Indian and P[8] Rotateq VP8*s formed only hydrophobic interactions with Gal4. Residue 216 also appeared to be genotype specific, being N216, N216, V216, T216 in P[8], P[4], P[6], and P[19], respectively, playing various roles. For example, N216 in P[4] and P[8] VP8* contributed a hydrogen bond with the GalII, T216 in P[19] VP8* formed a relatively weak hydrophobic interaction with GalII, while V216 in P[6] VP8* does not involved a direct interaction with LNFP1 (Fig. 5B right panel).

P[8] VP8*s Did Not Hemagglutinate the ABO Red Blood Cells

We then tested hemagglutination activity of the P[8] rotavirus VP8*s in form of GST-VP8* fusion proteins to human red blood cells of A, B, and O types. Rotateq P[8]/P[8]11221075/BELP[8] VP8*s did not hemagglutinate any of the A, B, and O type red blood cells (Fig. 6). The red blood cells of sheep, bovine, pig, and rabbit were also tested but again they were not hemagglutinated by Rotateq P[8] VP8*. Human P[4] and P[6] VP8*s did not show hemagglutination to A, B, O type cells either. As a positive control, the GST tagged P[14] VP8* that recognizes the A type HBGA in the *in vitro* assays hemagglutinated the A type red blood cells (Fig. 6).

Human Milk, LNFP1, and Core 2 Inhibited Cell Infection by P[8] Wa RV

Human milk, as well as oligosaccharides LNFP1, core 2, and lactose were used to inhibit P[8] Wa RV infection and replication in cultured MA104 cells (Fig. 7A, 7B). The fluorescent focus was seen as shown in Fig. 7A. P[8] Wa RV infection/replication reduced following incubation of the viruses with human milk at 1:10 (Fig. 7B). Similar blocking effects were observed by LNFP1 glycan at 5 μg/μL. LNFP1 and core 2 glycans at 1 μg/μL also displayed inhibition against P[8] Wa virus infection. Lactose (5 μg/μL) did not show such inhibition. SA11 RV infection was blocked by human milk but not inhibited by LNFP1.

Discussion

Since HBGA glycans were first reported as host attachment factors for RV infection in 2012 (Hu *et al.* 2012; Huang *et al.* 2012; Liu *et al.* 2012), numerous studies have been conducted to explore the complex interactions between the genetically diverse RVs and their polymorphic glycan ligands. These included the phenotypic/functional studies to understand the genotype-specific glycan binding patterns (Huang *et al.* 2012; Liu *et al.* 2012; Ramani *et al.* 2013; Ma *et al.* 2015; Liu *et al.* 2016; Jiang *et al.* 2017), the structural investigations to elucidate the molecular mechanisms

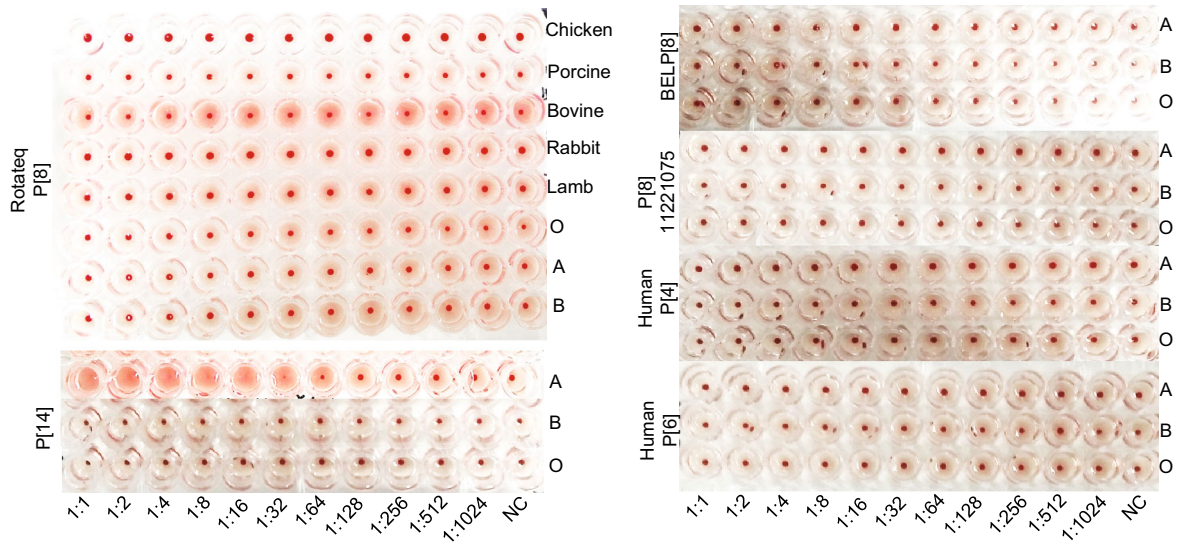

Fig. 6 Hemagglutination assay of the recombinant VP8* proteins. GST-VP8* proteins were serially diluted with PBS. Human A, B, O and animal blood cells were applied to the Rotateq P[8] assay. BELP[8], labP[8]-11221075, human P[4]-11151099, P[6]-5311142, P[14] VP8*s were analyzed using human A, B, O red blood cells.

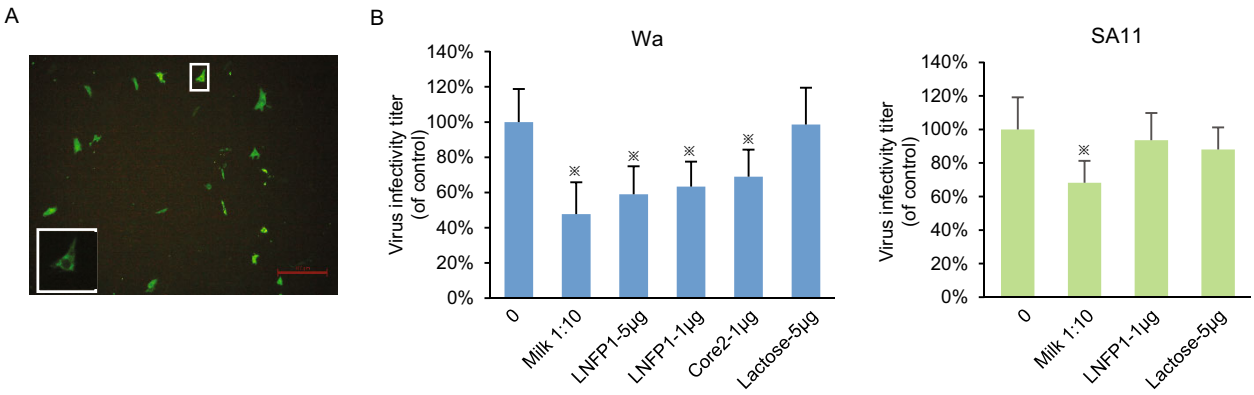

Fig. 7 Inhibition of P[8] Wa RV replication in cell culture by human milk and LNFPI/core 2 conjugates. SA11 virus was included as a control. **A** Representative immunofluorescence microscopy image of MA104 cells infected with P[8] Wa RV. Each green dot represents an infected cell, as shown in the enlarged panel. The red line is a scale bar of 100 μm. The plotted blocking results are shown in panels. **B** Each bar represents mean % infectivity, with no glycan treatment considered to be 100%. LNFPI, mucin core 2 and lactose oligosaccharides were used at final concentrations of 1 or 5 μg/μL. All assays were carried out twice, with triplicates within each experiment. Error bars represent standard error of the mean. *P*-values < 0.05 were considered statistically significant [analysis of variance (ANOVA) with Dunnett's correction for multiple comparisons]. The asterisk indicates a statistical difference of $P < 0.05$.

behind such interactions (Hu *et al*. 2012, 2015, 2018; Liu *et al*. 2017; Sun *et al*. 2018), and the epidemiology surveillance to associate the human HBGA phenotypes and their susceptibility to RV infection (Imbert-Marcille *et al*. 2014; Nordgren *et al*. 2014; Van Trang *et al*. 2014; Ayouni *et al*. 2015; Sun *et al*. 2016b; Barbe *et al*. 2018). Despite these many studies, our understanding of the globally predominant P[8] RVs in their glycan binding specificity and the mechanism behind virus-glycan binding remain limited. In this study, we verified that P[8] VP8* bound both mucin core 2 glycans and H type 1 antigen via oligosaccharide binding assays. More importantly, we solved the crystal structures of the Rotateq P[8] VP8* proteins complexed with a mucin core 2 trisaccharide and an H type 1 pentasaccharide, respectively, allowing elucidation of the structural basis and mechanism of P[8] RV-glycan ligand interactions.

P[8] and P[4] RVs are grouped into the P[II] genogroup together with P[6] and P[19] (Liu *et al*. 2012). P[4] and P[6] RVs are also predominant worldwide, next to the P[8] genotype and the structural basis of P[4]/P[6]/P[19] VP8* binding to H type 1 glycans have been determined previously, revealing a similar glycan binding site (Liu *et al*. 2017; Hu *et al*. 2018; Sun *et al*. 2018). Here, the crystal structures of P[8] VP8* in complex with core 2 trisaccharide and LNFP1 pentasaccharide verified that the P[8] glycan binding site is indeed highly conserved with the known ones of P[4], P[6], and P[19] VP8*s (Liu *et al*. 2017; Hu *et al*. 2018; Sun *et al*. 2018) in the P[II] genogroup, but not with those of other non-P[II] human RVs (Hu *et al*. 2012, 2015). We further noted that among the P[II] RVs the amino acids constituting the P[8] glycan binding site are identical to those of the P[4] RVs, while their homology is lower to those of P[19] and even further lower to those of human P[6] glycan binding sites, consistent with their phylogenic relationship (Liu *et al*. 2012; Hu *et al*. 2018). These observations may help our understanding on virus-host interaction and prevalence of the globally predominant P[8] RVs.

Our observations that VP8*s of three P[8] RV strains showed obvious binding to mucin core 2, were consistent with those observed previously (Liu *et al*. 2016). In fact, many tested VP8*s of the P[II] RVs, including human P[4], human P[19], porcine P[19], and porcine P[6] were found to bind mucin core 2 glycan, while human P[6] did not (Liu *et al*. 2016; Pang *et al*. 2018; Sun *et al*. 2018). Mucin core 2 glycans distribute in a variety of cells and tissues (Moran *et al*. 2011). Our virus inhibition assays showed that core 2 glycan inhibited P[8] RV infection, and similar inhibitory effect was observed to P[19] RV infection (Liu *et al*. 2017). These data suggested that mucin core glycans, especially core 2, may be important host attachment factors for the P[II] RVs. The structural superimposition and sequence alignment showed the amino acids involved in the interactions with core 2 trisaccharide were relatively conserved in all P[4]/P[8]/P[6]/P[19] RVs except for residue 169. Y169 that is conserved in P[4]/P[8] RVs formed different interactions with core 2 compared with H169 of other P genotypes, which may partly contribute to the differences in binding ability to core 2 glycans. In addition, P[10] VP8* of P[I] genogroup was also reported to recognize the mucin core 2 glycan and shared almost the same amino acids in the glycan binding site (Liu *et al*. 2016; Pang *et al*. 2018). Thus, further studies to clarify the specific roles of mucin cores in human RV host ranges and infection are necessary.

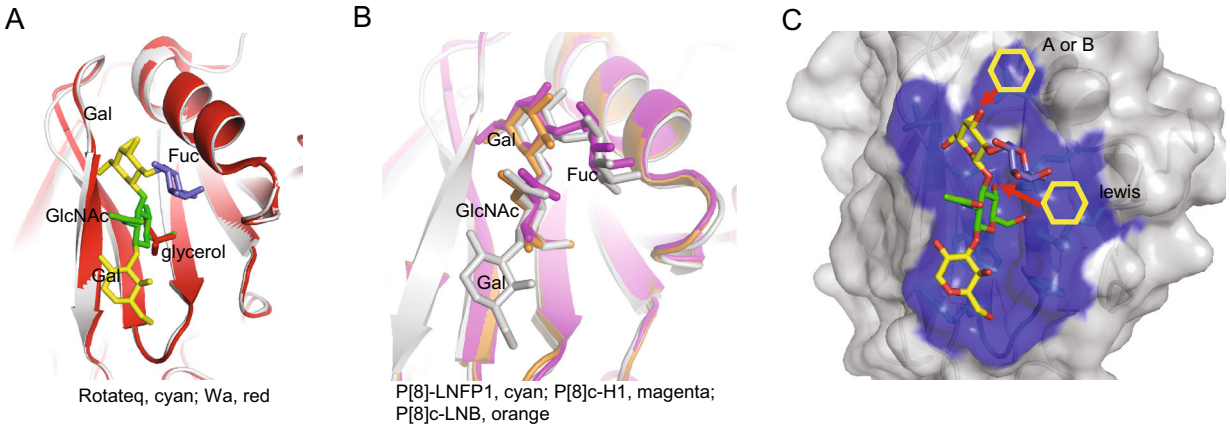

Fig. 8 **A** Structural superimposition of Rotateq P[8] VP8*-LNFP1 (PDB: 6K2O) and Wa P[8] VP8* (PDB: 2DWR). LNFP1 in Rotateq P[8] and the glycerol molecule in Wa P[8] were shown in stick. The LNFP1 was colored as described in Fig. 3. Glycerol was colored red. **B** Structural comparison of Rotateq P[8] VP8*-LNFP1 (PDB: 6K2O, gray), $P[8]_c$ VP8*-H1 (PDB: 6HA0, magenta), $P[8]_c$ VP8*-LNB (PDB: 6H9Y, orange). LNFP1, H1, and LNB were presented in stick with color of gray, magenta, orange, respectively. **C** Surface presentation of LNFP1 binding site in Rotateq P[8] VP8* and the supposed elongation of A/B/lewis antigens.

Our study confirmed that P[8] VP8* recognize H type 1 antigen (Huang *et al*. 2012; Ma *et al*. 2015), but such interaction may be weak. For example, P[8]11221075 VP8* bound conclusively to H type 1 antigens, while the other tested P[8] VP8*s appeared to bind much weaker. P[8] and P[4] VP8*s bound LNT (Galβ1-3GlcNAcβ1-3Galβ1-4Glc) weakly although this glycan contains the H type 1 sequences with one fucose less compared with LNFP1, while P[6] VP8* bound LNT strongly, consistent with a previous study (Liu *et al*. 2016). Sequence and structural analysis showed that four specific amino acids of P[6] VP8*, spanning from 169 to172 that build part of the glycan binding site, interact strongly with Galβ1-4Glc of LNFP1 at the reducing end, while only relative weak hydrophobic interactions are seen in the P[8]/P[4] VP8*-glycan structures with Glc pointing away from the binding cavity (Fig. 5B). These structural variations explain at least partially the difference of the binding intensity. For the P[19]-LNFP1 complex structure, H169 also formed hydrogen bonds with Gal4 of LNFP1, partially contributing to the relatively strong binding intensity between P[19] and LNFP1/LNT (Liu *et al*. 2016; Sun *et al*. 2018). Residue 216 was another amino acid that showed genotype-specific changes and contributed to various interactions in the genotype-related manner as described above, that is, N216 that is specific and relatively conserved in human P[8] and P[4] formed intense interactions with the LNFP1. We speculated that the amino acid variations such as residues 169 and 216 affect the binding intensity to different glycan ligands, which may play a part role in the human RV evolution and prevalence.

Rotateq P[8] RV VP8* bound to core 2 and H type 1 LNFP1 glycans using the same site. The native crystal structure of P[8] Wa was solved previously (Blanchard *et al*. 2007). Rotateq VP8* structure is close to Wa P[8] VP8* with the RMSD value of 0.277. Interestingly, a glycerol molecule was found in P[8] Wa VP8* at the position equivalent to the GlcNAc of LNFP1 binding site of Rotateq VP8* (Fig. 8A), showing that the P[8] glycan binding site can bind different ligands exquisitely. A recent paper reported the complex structures of $P[8]_c$ VP8* with type I precursor (LNB, Galβ1-3GlcNAc) and H type 1 (H1, Fucα1-2Galβ1-3GlcNAc) (Rey *et al*. 2019). We noted that VP8* bound to the glycans via the same site (Fig. 8B). Compared to the structure of P[8] VP8*-LNFP1, LNB and H1 located exactly the position of LNFP1 (Fig. 8B), indicating that P[8] VP8* can accommodate various type I related glycans. Previous studies suggested that P[19] VP8*s bind glycans using the GlcNAcβ1-3Gal as the basic functional unit (Liu *et al*. 2017; Sun *et al*. 2018), which appear the same case in P[8] RV, suggesting that this may be the basic property of all P[II] RVs to bind the GlcNAc-containing glycans. Furthermore, while the GlcNAc-binding pocket was conserved among P[II] RVs, the P[II] RV genotypes exhibited a genotype-specific difference in recognizing the mucin core and type 1-related sequences as shown in our and other studies (Liu *et al*. 2017; Hu *et al*. 2018; Sun *et al*. 2018).

The type 1 precursor Galβ1-3GlcNAc could develop into different H, A, B, and Lewis HBGAs by adding one specific saccharide step by step. Interestingly, P[8] RV VP8* did not interact with A/B/Lewis type HBGAs as shown by both oligosaccharide binding and red blood cell hemagglutination assays. The binding of P[8] VP8*s to saliva samples was independent on the ABO types (Sun *et al*. 2016a). In addition, two previous epidemiological studies found that P[8] RV infect preferably secretors irrespective of the individual's ABO types (Van Trang

et al. 2014; Sun *et al*. 2016c), while another recent study demonstrated that *in vitro* infection of transformed cell lines by P[8] RVs was independent of HBGAs expression (Barbe *et al*. 2018). These results supported the notion that P[8] RV VP8* may not recognize the ABO HBGAs. Structural analysis showed that a linkage of a GalNAc (A) or a Gal (B) to the O3 of GalII is sterically possible, but an addition of fucose to GlcNAc by α1-4 linkage to generate the Lewis antigens would cause steric hindrance (Fig. 8C). This may partly contribute to the fact that P[8] RV VP8* did not show obvious binding to a Lewis antigen in the oligosaccharide assay. Another possibility is that the binding to ABO HBGAs by P[8] VP8* may be too weak to be detected by an ELISA assay. A recent study using NMR titration experiments and NMR derived high ambiguity driven docking (HADDOCK) methods demonstrated that P[8] VP8* bound the Lewis b antigen with a Kd value of 43.4 mM via an undescribed pocket formed by two β-sheets (Xu *et al*. 2019). Further studies to clarify these issues are expected.

The available data indicate that all P[8], P[4], P[6], and P[19] interact with type I HBGA pentasaccharide LNFP1 that is a main component of the human milk oligosaccharides (HMOs) (Kunz *et al*. 2000). HMOs are believed to contain prebiotic or anti-microbial effector molecules benefiting neonates (Etzold and Bode 2014; Morozov *et al*. 2018). Accordingly, the VP8*s of human neonatal RVs (P[11]) bound HMOs independent from sialic acids, exhibiting a unique glycan specifically (Yu *et al*. 2014). Here, we showed that human P[8] VP8* recognized the HMO LNFP1 via the same binding mode as that of P[4]/P[6]/P[19] VP8*s. We and others (Liu *et al*. 2017; Hu *et al*. 2018) further showed that LNFP1 glycan inhibited infections of human P[8]/P[4]/P[6]/P[19] RVs infection, suggesting that LNFP1 glycans in the human milk may serve as decoy ligands to block the infectivity of human RVs, including P[8]/P[4]/P[6]. This may partly contribute to the reduced risk of breast-fed infants to acquire RV infection. However, a recent report showed that HMOs are not decoy receptors for G10P[11] and specific HMOs enhanced the infectivity of the neonatal-derived RV vaccine (P[11]), while HMOs had no significant effect on the infectivity of the globally dominant P[4] and P[8] human RVs (Ramani *et al*. 2018). These data discrepancies indicate the RV-HMOs interactions are complex and need further studies for clarification.

In summary, we have redefined the glycan binding specificity of the globally predominant P[8] RVs to verify the mucin core 2 as well as the H type I antigen as host ligands. Compared to that of Hu *et al*. (2018) which reported the P[4]/P[6] VP8*-LNFP1 structures, we determined the structure of P[8] VP8*-LNFP1, verifying the glycan binding site and interaction mechanism for P[8] RVs. For Rey *et al*. (2019) that determined P[8] VP8* in complex with H type 1 antigens, we demonstrated that P[8] VP8* not only interact with H type 1 antigens, but also mucin core antigens based on crystal structures of VP8*-LNFP1 and VP8*-core 2. Our study elucidated the structural basis of P[8] VP8* accommodating different glycan ligands and provided phenotypic and structural information to comprehensively understand the virus-host interaction and epidemiology of the globally prevalent P[8].

Acknowledgments We are grateful to Jingyu Yan in Dalian Institute of Chemical Physics for kindly providing the free LNFP1 oligosaccharide purified from human milk. We would like to thank George F. Gao, Jinhua Yan, and Yi Shi in the Institute of Microbiology for the help in data analysis. We thank Huiying Li, Xiaohui Gao, Qiuyu Huang, Yu Qing, Lili Pang, Miao Jin, Xiangyu Kong in our lab for their help in the experiments. We appreciate the help of Yuan Yuan, Min Zhao, Yan Li, Xu Yang, Ruchao Peng, and Han Wang in the Institute of Microbiology in X-ray data collection. The assistance by the staff at the Shanghai Synchrotron Radiation Facility (SSRF-beamline 17U) is acknowledged. This research was supported by grants from the National Science and Technology Major Project (2018ZX10711-001) and the National Natural Science Foundation of China (NSFC) (No. 81601813).

Author Contributions ZD, XS, and DL designed the experiments. XS, LD, DL, and MW performed the protein expression and glycan binding experiments. XS, LD, QZ, and HW performed the virus inhibition assay. JQ solved the structures. XS and JQ analyzed the structural data. XS, RB, WC interpreted the glycan binding data. XS wrote the draft manuscript. ZD, XS, and MT revised the manuscript.

Compliance with Ethical Statements

Conflict of interest The authors declare that they have no conflict of interest.

Animal and Human Rights Statement The study was approved by the Medical Ethics Committee at National Institute for Viral Disease Control and Prevention, China CDC, Beijing, China and by the Institutional Animal Care and Use Committee (IACUC) of National Institute for Viral Disease Control and Prevention, China CDC. All the experimental procedures were performed in accordance with the Regulations for the Administration of Affairs Concerning Experimental Animals approved by the State Council of People's Republic of China.

References

Adams PD, Afonine PV, Bunkoczi G, Chen VB, Davis IW, Echols N, Headd JJ, Hung LW, Kapral GJ, Grosse-Kunstleve RW, McCoy AJ, Moriarty NW, Oeffner R, Read RJ, Richardson DC, Richardson JS, Terwilliger TC, Zwart PH (2010) PHENIX: a comprehensive python-based system for macromolecular structure solution. Acta Crystallogr D Biol Crystallogr 66:213–221

Ayouni S, Sdiri-Loulizi K, de Rougemont A, Estienney M, Ambert-Balay K, Aho S, Hamami S, Aouni M, Neji-Guediche M, Pothier P, Belliot G (2015) Rotavirus P[8] infections in persons with secretor and nonsecretor phenotypes, Tunisia. Emerg Infect Dis 21:2055–2058

Barbe L, Le Moullac-Vaidye B, Echasserieau K, Bernardeau K, Carton T, Bovin N, Nordgren J, Svensson L, Ruvoen-Clouet N, Le Pendu J (2018) Histo-blood group antigen-binding specificities of human rotaviruses are associated with gastroenteritis but not with *in vitro* infection. Sci Rep 8:12961

Blanchard H, Yu X, Coulson BS, von Itzstein M (2007) Insight into host cell carbohydrate-recognition by human and porcine rotavirus from crystal structures of the virion spike associated carbohydrate-binding domain (VP8*). J Mol Biol 367:1215–1226

Bohm R, Fleming FE, Maggioni A, Dang VT, Holloway G, Coulson BS, von Itzstein M, Haselhorst T (2015) Revisiting the role of histo-blood group antigens in rotavirus host-cell invasion. Nat Commun 6:5907

Burnett E, Parashar U, Tate J (2018) Rotavirus vaccines: effectiveness, safety, and future directions. Paediatr Drugs 20:223–233

Ciarlet M, Estes MK (1999) Human and most animal rotavirus strains do not require the presence of sialic acid on the cell surface for efficient infectivity. J Gen Virol 80(Pt 4):943–948

Desselberger U (2017) Differences of rotavirus vaccine effectiveness by country: likely causes and contributing factors. Pathogens. https://doi.org/10.3390/pathogens6040065

Dormitzer PR, Sun ZY, Wagner G, Harrison SC (2002) The rhesus rotavirus VP4 sialic acid binding domain has a galectin fold with a novel carbohydrate binding site. EMBO J 21:885–897

Emsley P, Cowtan K (2004) Coot: model-building tools for molecular graphics. Acta Crystallogr D Biol Crystallogr 60:2126–2132

Estes MK, Greenberg HB (2013) Rotaviruses. In: Knipe DM, Howley PM et al (eds) Fields Virology, 6th edn. Wolters Kluwer Health/Lippincott Williams & Wilkins, Philadelphia, pp 1347–1401

Etzold S, Bode L (2014) Glycan-dependent viral infection in infants and the role of human milk oligosaccharides. Curr Opin Virol 7:101–107

Fiore L, Greenberg HB, Mackow ER (1991) The VP8 fragment of VP4 is the rhesus rotavirus hemagglutinin. Virology 181:553–563

Fleming FE, Bohm R, Dang VT, Holloway G, Haselhorst T, Madge PD, Deveryshetty J, Yu X, Blanchard H, von Itzstein M, Coulson BS (2014) Relative roles of GM1 ganglioside, N-acylneuraminic acids, and α2β1 integrin in mediating rotavirus infection. J Virol 88:4558–4571

Gunaydin G, Nordgren J, Sharma S, Hammarstrom L (2016) Association of elevated rotavirus-specific antibody titers with HBGA secretor status in Swedish individuals: the FUT2 gene as a putative susceptibility determinant for infection. Virus Res 211:64–68

Haselhorst T, Fleming FE, Dyason JC, Hartnell RD, Yu X, Holloway G, Santegoets K, Kiefel MJ, Blanchard H, Coulson BS, von Itzstein M (2009) Sialic acid dependence in rotavirus host cell invasion. Nat Chem Biol 5:91–93

Hu L, Crawford SE, Czako R, Cortes-Penfield NW, Smith DF, Le Pendu J, Estes MK, Prasad BV (2012) Cell attachment protein VP8* of a human rotavirus specifically interacts with A-type histo-blood group antigen. Nature 485:256–259

Hu L, Ramani S, Czako R, Sankaran B, Yu Y, Smith DF, Cummings RD, Estes MK, Venkataram Prasad BV (2015) Structural basis of glycan specificity in neonate-specific bovine-human reassortant rotavirus. Nat Commun 6:8346

Hu L, Sankaran B, Laucirica DR, Patil K, Salmen W, Ferreon ACM, Tsoi PS, Lasanajak Y, Smith DF, Ramani S, Atmar RL, Estes MK, Ferreon JC, Prasad BVV (2018) Glycan recognition in globally dominant human rotaviruses. Nat Commun 9:2631

Huang P, Xia M, Tan M, Zhong W, Wei C, Wang L, Morrow A, Jiang X (2012) Spike protein VP8* of human rotavirus recognizes histo-blood group antigens in a type-specific manner. J Virol 86:4833–4843

Imbert-Marcille BM, Barbe L, Dupe M, Le Moullac-Vaidye B, Besse B, Peltier C, Ruvoen-Clouet N, Le Pendu J (2014) A FUT2 gene common polymorphism determines resistance to rotavirus A of the P[8] genotype. J Infect Dis 209:1227–1230

Jensen PH, Kolarich D, Packer NH (2010) Mucin-type O-glycosylation—putting the pieces together. FEBS J 277:81–94

Jiang X, Liu Y, Tan M (2017) Histo-blood group antigens as receptors for rotavirus, new understanding on rotavirus epidemiology and vaccine strategy. Emerg Microbes Infect 6:e22

Johannes M, Reindl M, Gerlitzki B, Schmitt E, Hoffmann-Roder A (2015) Synthesis and biological evaluation of a novel MUC1 glycopeptide conjugate vaccine candidate comprising a 4′-deoxy-4′-fluoro-Thomsen-Friedenreich epitope. Beilstein J Org Chem 11:155–161

Kuhlenschmidt TB, Hanafin WP, Gelberg HB, Kuhlenschmidt MS (1999) Sialic acid dependence and independence of group A rotaviruses. Adv Exp Med Biol 473:309–317

Kunz C, Rudloff S, Baier W, Klein N, Strobel S (2000) Oligosaccharides in human milk: structural, functional, and metabolic aspects. Annu Rev Nutr 20:699–722

Liu Y, Huang P, Tan M, Liu Y, Biesiada J, Meller J, Castello AA, Jiang B, Jiang X (2012) Rotavirus VP8*: phylogeny, host range, and interaction with histo-blood group antigens. J Virol 86:9899–9910

Liu Y, Huang P, Jiang B, Tan M, Morrow AL, Jiang X (2013) Poly-LacNAc as an age-specific ligand for rotavirus P[11] in neonates and infants. PLoS ONE 8:e78113

Liu Y, Ramelot TA, Huang P, Liu Y, Li Z, Feizi T, Zhong W, Wu FT, Tan M, Kennedy MA, Jiang X (2016) Glycan specificity of P[19] rotavirus and comparison with those of related P genotypes. J Virol 90:9983–9996

Liu Y, Xu S, Woodruff AL, Xia M, Tan M, Kennedy MA, Jiang X (2017) Structural basis of glycan specificity of P[19] VP8*: implications for rotavirus zoonosis and evolution. PLoS Pathog 13:e1006707

Ma X, Li DD, Sun XM, Guo YQ, Xiang JY, Wang WH, Zhang LX, Gu QJ, Duan ZJ (2015) Binding patterns of rotavirus genotypes P[4], P[6], and P[8] in China with histo-blood group antigens. PLoS ONE 10:e0134584

Matthijnssens J, Ciarlet M, McDonald SM, Attoui H, Banyai K, Brister JR, Buesa J, Esona MD, Estes MK, Gentsch JR, Iturriza-Gomara M, Johne R, Kirkwood CD, Martella V, Mertens PP, Nakagomi O, Parreno V, Rahman M, Ruggeri FM, Saif LJ, Santos N, Steyer A, Taniguchi K, Patton JT, Desselberger U, Van Ranst M (2011) Uniformity of rotavirus strain nomenclature proposed by the Rotavirus Classification Working Group (RCWG). Arch Virol 156:1397–1413

Moran AP, Gupta A, Joshi L (2011) Sweet-talk: role of host glycosylation in bacterial pathogenesis of the gastrointestinal tract. Gut 60:1412–1425

Morozov V, Hansman G, Hanisch FG, Schroten H, Kunz C (2018) Human milk oligosaccharides as promising antivirals. Mol Nutr Food Res 62:e1700679

Nordgren J, Sharma S, Bucardo F, Nasir W, Gunaydin G, Ouermi D, Nitiema LW, Becker-Dreps S, Simpore J, Hammarstrom L, Larson G, Svensson L (2014) Both lewis and secretor status mediate susceptibility to rotavirus infections in a rotavirus genotype dependent manner. Clin Infect Dis 59:1567–1573

Otwinowski Z, Minor W (1997) Processing of X-ray diffraction data collected in oscillation mode. Macromol Crystallogr Pt A 276:307–326

Pang LL, Wang MX, Sun XM, Yuan Y, Qing Y, Xin Y, Zhang JY, Li DD, Duan ZJ (2018) Glycan binding patterns of human rotavirus P[10] VP8* protein. Virol J 15:161

Pindyck T, Tate JE, Parashar UD (2018) A decade of experience with rotavirus vaccination in the United States—vaccine uptake, effectiveness, and impact. Expert Rev Vaccines 17:593–606

Pollock L, Bennett A, Jere KC, Dube Q, Mandolo J, Bar-Zeev N, Heyderman RS, Cunliffe NA, Iturriza-Gomara M (2018) Non-secretor histo-blood group antigen phenotype is associated with reduced risk of clinical rotavirus vaccine failure in Malawian infants. Clin Infect Dis. https://doi.org/10.1093/cid/ciy1067

Ramani S, Cortes-Penfield NW, Hu L, Crawford SE, Czako R, Smith DF, Kang G, Ramig RF, Le Pendu J, Prasad BV, Estes MK (2013) The VP8* domain of neonatal rotavirus strain G10P[11] binds to type II precursor glycans. J Virol 87:7255–7264

Ramani S, Stewart CJ, Laucirica DR, Ajami NJ, Robertson B, Autran CA, Shinge D, Rani S, Anandan S, Hu L, Ferreon JC, Kuruvilla KA, Petrosino JF, Venkataram Prasad BV, Bode L, Kang G, Estes MK (2018) Human milk oligosaccharides, milk microbiome and infant gut microbiome modulate neonatal rotavirus infection. Nat Commun 9:5010

Read RJ (2001) Pushing the boundaries of molecular replacement with maximum likelihood. Acta Crystallogr D Biol Crystallogr 57:1373–1382

Rey FA, Gozalbo-Rovira R, Ciges-Tomas JR, Vila-Vicent S, Buesa J, Santiso-Bellón C, Monedero V, Yebra MJ, Marina A, Rodríguez-Díaz J (2019) Unraveling the role of the secretor antigen in human rotavirus attachment to histo-blood group antigens. PLoS Pathog 15:e1007865

Rha B, Tate JE, Payne DC, Cortese MM, Lopman BA, Curns AT, Parashar UD (2014) Effectiveness and impact of rotavirus vaccines in the United States—2006–2012. Expert Rev Vaccines 13:365–376

Ruggeri FM, Greenberg HB (1991) Antibodies to the trypsin cleavage peptide VP8 neutralize rotavirus by inhibiting binding of virions to target cells in culture. J Virol 65:2211–2219

Skovlund VR (1997) ABH and related histo-blood group antigens in normal & malignant human endometrium in relation to genetic and hormonal factors. APMIS Suppl 69:1–33

Sun X, Guo N, Li D, Jin M, Zhou Y, Xie G, Pang L, Zhang Q, Cao Y, Duan ZJ (2016a) Binding specificity of P[8] VP8* proteins of rotavirus vaccine strains with histo-blood group antigens. Virology 495:129–135

Sun X, Guo N, Li J, Yan X, He Z, Li D, Jin M, Xie G, Pang L, Zhang Q, Liu N, Duan ZJ (2016b) Rotavirus infection and histo-blood group antigens in the children hospitalized with diarrhoea in China. Clin Microbiol Infect 22(740):e741–e743

Sun X, Guo N, Li J, Yan X, He Z, Li D, Jin M, Xie G, Pang L, Zhang Q, Liu N, Duan ZJ (2016c) Rotavirus infection and histo-blood group antigens in the children hospitalized with diarrhoea in China. Clin Microbiol Infect. https://doi.org/10.1016/j.cmi.2016.06.007

Sun X, Li D, Peng R, Guo N, Jin M, Zhou Y, Xie G, Pang L, Zhang Q, Qi J, Duan ZJ (2016d) Functional and structural characterization of P[19] rotavirus VP8* Interaction with histo-blood group antigens. J Virol 90:9758–9765

Sun X, Li D, Qi J, Chai W, Wang L, Wang L, Peng R, Wang H, Zhang Q, Pang L, Kong X, Wang H, Jin M, Gao GF, Duan Z (2018) Glycan binding specificity and mechanism of human and porcine P[6]/P[19] rotavirus VP8*s. J Virol 92:e00538-18

Tan M, Jiang X (2014) Histo-blood group antigens: a common niche for norovirus and rotavirus. Expert Rev Mol Med 16:e5

Tate JE, Burton AH, Boschi-Pinto C, Parashar UD, World Health Organization-Coordinated Global Rotavirus Surveillance N (2016) Global, regional, and national estimates of rotavirus mortality in children < 5 years of age, 2000–2013. Clin Infect Dis 62(Suppl 2):S96–S105

Van Trang N, Vu HT, Le NT, Huang P, Jiang X, Anh DD (2014) Association between norovirus and rotavirus infection and histo-blood group antigen types in Vietnamese children. J Clin Microbiol 52:1366–1374

Xu S, Liu Y, Tan M, Zhong W, Zhao D, Jiang X, Kennedy MA (2019) Molecular basis of P[6] and P[8] major human rotavirus VP8* domain interactions with histo-blood group antigens. BioRxiv. https://doi.org/10.1101/512301:512301

Yu Y, Lasanajak Y, Song X, Hu L, Ramani S, Mickum ML, Ashline DJ, Prasad BV, Estes MK, Reinhold VN, Cummings RD, Smith DF (2014) Human milk contains novel glycans that are potential decoy receptors for neonatal rotaviruses. Mol Cell Proteom 13:2944–2960

Yu J, Lai S, Geng Q, Ye C, Zhang Z, Zheng Y, Wang L, Duan Z, Zhang J, Wu S, Parashar U, Yang W, Liao Q, Li Z (2018) Prevalence of rotavirus and rapid changes in circulating rotavirus strains among children with acute diarrhea in China, 2009–2015. J Infect. https://doi.org/10.1016/j.jinf.2018.07.004

Zhang XF, Long Y, Tan M, Zhang T, Huang Q, Jiang X, Tan WF, Li JD, Hu GF, Tang S, Dai YC (2016) P[8] and P[4] rotavirus infection associated with secretor phenotypes among children in South China. Sci Rep 6:34591